Guided Waves in Functionally Graded Rods with Rectangular Cross-Section under Initial Stress

Xiaoming Zhang[1], Jiangong Yu[1,2], Min Zhang[1], Dengpan Zhang[1]

Abstract: The characteristics of the guided waves propagation in functionally graded rods with rectangular cross-section (finite width and height) under initial stress are investigated in this paper based on Biot's theory of incremental deformation. An extended orthogonal polynomial approach is present to solve the coupled wave equations with variable coefficients. By comparisons with the available results of a rectangular aluminum rod, the validity of the present approach is illustrated. The dispersion curves and displacement profiles of various rectangular functionally graded rods are calculated to reveal the wave characteristics, and the effects of different width to height ratios and initial stress and gradient functions on the guided waves are discussed in detail.

Keywords: Guided waves; Initial stress; Rectangular rod; Functionally graded materials; Orthogonal polynomial approach; Dispersion curves.

1   Introduction

Functionally graded materials (FGM) are advanced composites consisting of two or more material phases whose mechanical properties vary continuously throughout the volume depending on spatial coordinates. Owing to their great advantages, Functionally graded materials have been known to have extensive applications in many fields, such as electronics, aerospace, protection industries and so on. For the purpose of the guided ultrasonic non-destructive testing and evaluation (NDTE), the guided wave propagation in FGM structures has received considerable research efforts. As early as more than twenty years ago, wave propagation in FGM plates was investigated [Liu, Tani, and Ohyoshi (1991)]. Later on, guided wave in FGM structures was investigated by various methods, such as the linearly inhomogeneous elements and quadratic layer elements methods [Han, Liu, and Lam (2000); Han

---

[1] School of Mechanical and Power Engineering, Henan Polytechnic University, Jiaozuo 454000, P.R. China.

[2] Corresponding Author. E-mail: yuee@hpu.edu.cn

and Liu (2003)], spectral finite element method [Chakraborty and Gopalakrishnan (2004); Bishay, Sladek, Sladek, and Atluri (2012)], Galerkin finite element and Newmark methods [Hosseini (2009)], reverberation matrix method [Chen, Wang, and Bao (2007); Zhu, Yang, and Kitipornchai (2013)], and so on.

All the above-mentioned methods were to separate FGM structures into some homogeneous or inhomogeneous layers. Many other research works treated FGM structures as continuously graded media [Sun and Luo (2011); Xue and Pan (2013), Moussavinezhad, Shahabian, and Hosseini (2013)]. Lefebvre et al. developed a Legendre polynomial series method to investigate wave propagation in various FGM structures [Lefebvre, Zhang, Gazalet, Gryba, and Sadaune (2001); Elmaimouni, Lefebvre, Zhang, and Gryba (2005)]. The specificity of the polynomial series method resides on how the boundary conditions are incorporated into the motion equations and are automatically accounted for the deviece by assuming position-dependent material parameters. Then the motion equations are converted into a matrix eigenvalue problem through the expansion of the independent mechanical variables into appropriate series of orthonormal functions. By using the polynomial series method, Yu et al. investigated the guided wave characteristics in FGM spherical plates and viscoelastic FGM plates [Yu, Wu, and He (2007); Yu, Ratolojanahary, and Lefebvre (2011)]. Recently, Liu et al. studied the elastic wave in FGM bars by the Rayleigh-Ritz method based on two dimensional Legendre polynomial [Liu, Han, Huang, Li, Liu, and Wu (2015)]. However, in all the above-mentioned researches, the initial stress induced during the processing was not taken into account.

Due to the limitation of the manufacturing technology, the presence of initial stress in FGM is unavoidable. It is well known that initial stress can affect mechanical behaviors of the structures significantly. So it is meaningful to study the effect of the stress on the wave propagation in functionally graded materials and structures, and some investigations have been done by Abd-Alla and Ahmed (1999); Qian, Jin, Lu, Kishimoto, and Hirose (2010); Saroj, Sahu, Chaudhary, and Chattopadhyay (2015) and many others. But most studies focused on Love-waves in FGM half-space. Recently, taking into account the effect of the initial stress, Yu et al. investigated the guided waves in some one-dimensional structures, i.e., structures having the finite dimension in only one direction, such as axially infinite hollow cylinders [Yu and Zhang (2013)] and horizontally infinite flat plates [Yu and Zhang (2014)]. However, few investigations on the effect of the initial stress on the wave propagation in two-dimensional structures having the finite dimension in two directions,such as square rods, rings and so on, have been reported.

In this paper, based on Biot's theory of incremental deformation [Biot (1965)], we study the guided wave characteristics in rectangular FGM rods under initial stress

by an extended polynomial approach. Through numerical comparisons with the available results, the validation of the present polynomial approach is illustrated. The dispersion curves and displacement profiles of various rectangular FGM rods are obtained, and the effects of different width to height ratios and initial stress and gradient functions on the guided wave charateristics are illustrated.

2 Mathematical formulation of the problem

Considering an orthotropic FGM rectangular rod with initial stress, as shown in Fig. 1. The material properties vary continuously across z direction. The rod is infinite in the wave propagating direction (x-axis) and the compressive stress is $S_{xx} = -P$ and width is d and height h. The origin of the Cartesian coordinate system is located at the corner of the rectangular cross section and the rod lies in the positive y-z region, where the cross-section is defined by the region $0 \leq z \leq h$ and $0 \leq y \leq d$.
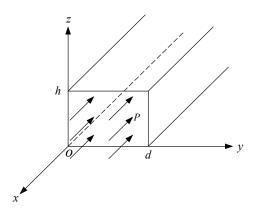

Figure 1: Schematic of a rod with a rectangular cross section.

According to "Mechanics of Incremental Deformations", the dynamic equation for the unidirectional composite rod under gravity and initial stress is governed by

$$\frac{\partial T_{xx}}{\partial x} + \frac{\partial T_{xy}}{\partial y} + \frac{\partial T_{xz}}{\partial z} - \frac{1}{2}\left(\frac{\partial u_x}{\partial z} + \frac{\partial u_z}{\partial x}\right)\frac{\partial S_{xx}}{\partial z} + S_{xx}\frac{\partial \omega_z}{\partial y} - S_{xx}\frac{\partial \omega_y}{\partial z} = \rho\frac{\partial^2 u_x}{\partial t^2}$$

$$\frac{\partial T_{xy}}{\partial x} + \frac{\partial T_{yy}}{\partial y} + \frac{\partial T_{yz}}{\partial z} + S_{xx}\frac{\partial \omega_z}{\partial x} = \rho\frac{\partial^2 u_y}{\partial t^2} \qquad (1)$$

$$\frac{\partial T_{xz}}{\partial x} + \frac{\partial T_{yz}}{\partial y} + \frac{\partial T_{zz}}{\partial z} - S_{xx}\frac{\partial \omega_y}{\partial x} = \rho\frac{\partial^2 u_z}{\partial t^2}$$

where $\omega_x = \frac{1}{2}\left(\frac{\partial u_z}{\partial y} - \frac{\partial u_y}{\partial z}\right)$, $\omega_y = \frac{1}{2}\left(\frac{\partial u_x}{\partial z} - \frac{\partial u_z}{\partial x}\right)$, $\omega_z = \frac{1}{2}\left(\frac{\partial u_y}{\partial x} - \frac{\partial u_x}{\partial y}\right)$, and T_{ij}, u_i

and ρ are respectively the stress and the displacement components and the mass density of the material.

The strain-displacement relationships are:

$$\varepsilon_{xx} = \frac{\partial u_x}{\partial x}, \ \varepsilon_{yy} = \frac{\partial u_y}{\partial y}, \ \varepsilon_{zz} = \frac{\partial u_z}{\partial z}, \ \varepsilon_{yz} = \frac{1}{2}\left(\frac{\partial u_y}{\partial z} + \frac{\partial u_z}{\partial y}\right),$$

$$\varepsilon_{xz} = \frac{1}{2}\left(\frac{\partial u_x}{\partial z} + \frac{\partial u_z}{\partial x}\right), \ \varepsilon_{xy} = \frac{1}{2}\left(\frac{\partial u_x}{\partial y} + \frac{\partial u_y}{\partial x}\right). \tag{2}$$

where ε_{ij} are the strain components.

The constitutive equation can be written in the following form:

$$\begin{Bmatrix} T_{xx} \\ T_{yy} \\ T_{zz} \\ T_{yz} \\ T_{xz} \\ T_{xy} \end{Bmatrix} = \begin{bmatrix} C_{11} - S_{xx} & C_{12} - S_{xx} & C_{13} - S_{xx} & 0 & 0 & 0 \\ C_{12} & C_{22} & C_{23} & 0 & 0 & 0 \\ C_{13} & C_{23} & C_{33} & 0 & 0 & 0 \\ 0 & 0 & 0 & C_{44} & 0 & 0 \\ 0 & 0 & 0 & 0 & C_{55} & 0 \\ 0 & 0 & 0 & 0 & 0 & C_{66} \end{bmatrix} \begin{Bmatrix} \varepsilon_{xx} \\ \varepsilon_{yy} \cdot \mathrm{I}(y,z) \\ \varepsilon_{zz} \cdot \mathrm{I}(y,z) \\ 2\varepsilon_{yz} \cdot \mathrm{I}(y,z) \\ 2\varepsilon_{xz} \cdot \mathrm{I}(y,z) \\ 2\varepsilon_{xy} \cdot \mathrm{I}(y,z) \end{Bmatrix} \tag{3}$$

where C_{ij} are the elastic coefficients, and $\mathrm{I}(y,z)$ is the rectangular window function, which is introduced so as to meet the stress-free boundary conditions ($T_{zz} = T_{xz} = T_{yz} = T_{yy} = T_{xy} = 0$ at the four boundaries) and defined as

$$\mathrm{I}(y,z) = \begin{cases} 1, & 0 \leq y \leq d \text{ and } 0 \leq z \leq h \\ 0, & elsewhere \end{cases} \tag{4}$$

Since the material properties vary in the z-direction, the elastic parameters of the rod are functions of z, which can expressed as

$$C_{ij}(z) = C_{ij}^{(0)} + C_{ij}^{(1)}\left(\frac{z}{h}\right)^1 + C_{ij}^{(2)}\left(\frac{z}{h}\right)^2 + \cdots + C_{ij}^{(L)}\left(\frac{z}{h}\right)^L.$$

With implicit summation over repeated indices, $C_{ij}(z)$ can be written compactly as

$$C_{ij}(z) = C_{ij}^{(l)}\left(\frac{z}{h}\right)^l, \ l = 0,1,2\ldots,L. \tag{5a}$$

Similarly, the mass density can be represented by

$$\rho(z) = \rho^{(l)}\left(\frac{z}{h}\right)^l, \ l = 0,1,2\ldots,L. \tag{5b}$$

For plane time-harmonic wave propagating in the *x*-direction of a rectangular rod, we assume the displacement components having the following form:

$$u_x(x,y,z,t) = \exp(\mathrm{i}kx - \mathrm{i}\omega t)U(y,z) \tag{6a}$$

$$u_y(x,y,z,t) = \exp(\mathrm{i}kx - \mathrm{i}\omega t)V(y,z) \tag{6b}$$

$$u_z(x,y,z,t) = \exp(\mathrm{i}kx - \mathrm{i}\omega t)W(y,z) \tag{6c}$$

where $U(y,z)$, $V(y,z)$ and $W(y,z)$ represent the wave amplitudes in the *x*-, *y*- and *z*-directions respectively. *k* is the magnitude of the wave vector in the propagation direction and ω is the angular frequency.

Substituting Eqs. (2), (4), (5) and (6) into Eq. (1), we can obtain the governing differential equations in terms of the displacement components:

$$\frac{z^l}{h^l}\left[C_{55}^{(l)}U_{,zz} - k^2 C_{11}^{(l)}U + C_{66}^{(l)}U_{,yy} + \mathrm{i}k(C_{12}^{(l)} + C_{66}^{(l)})V_{,y} + \mathrm{i}k(C_{13}^{(l)} + C_{55}^{(l)})W_{,z} + lz^{-1}C_{55}^{(l)}U_{,z}\right.$$

$$\left. + lz^{-1}C_{55}^{(l)}W\right]I(y,z) + \frac{z^l}{h^l}C_{55}^{(l)}(U_{,z} + \mathrm{i}kW)I(y,z) + \frac{z^l}{h^l}C_{66}^{(l)}(U_{,y} + \mathrm{i}kV)I(y,z)_{,y} \tag{7a}$$

$$+ 0.5P'(U_{,z} + \mathrm{i}kW)I(y,z) + P(0.5\mathrm{i}kV_{,y} + 0.5\mathrm{i}kW_{,z} - k^2 U + 0.5U_{,yy} + 0.5U_{,zz})I(y,z)$$

$$= -\frac{z^l \rho^{(l)}\omega^2 U}{h^l}I(y,z)$$

$$\frac{z^l}{h^l}\left[C_{44}^{(l)}V_{,zz} - k^2 C_{66}^{(l)}V + \mathrm{i}k(C_{12}^{(l)} + C_{66}^{(l)})U_{,y} + (C_{23}^{(l)} + C_{44}^{(l)})W_{,yz} + lz^{-1}C_{44}^{(l)}(V_{,z} + W_{,y})\right.$$

$$\left. + C_{22}^{(l)}V_{,yy}\right]I(y,z) + \frac{z^l}{h^l}C_{44}^{(l)}(V_{,z} + W_{,y})I(y,z)_{,z} + \frac{z^l}{h^l}\left(\mathrm{i}kC_{12}^{(l)}U + C_{22}^{(l)}V_{,y}\right. \tag{7b}$$

$$\left. + C_{23}^{(l)}W_{,z}\right)I(y,z)_{,y} + 0.5P(k^2 V + \mathrm{i}kU_{,y})I(y,z) = -\frac{z^l \rho^{(l)}\omega^2 V}{h^l}I(y,z)$$

$$\frac{z^l}{h^l}\left[C_{33}^{(l)}W_{,zz} - k^2 C_{55}^{(l)}W + C_{44}^{(l)}V_{,yy} + lz^l\left(\mathrm{i}kC_{13}^{(l)}U + C_{23}^{(l)}V_{,y} + C_{33}^{(l)}W_{,z}\right) + \mathrm{i}k(C_{13}^{(l)} + C_{55}^{(l)})\right.$$

$$\left. U_{,z} + (C_{23}^{(l)} + C_{44}^{(l)})W_{,yz}\right]I(y,z) + \frac{z^l}{h^l}\left(\mathrm{i}kC_{13}^{(l)}U + C_{23}V_{,y} + C_{33}^{(l)}W_{,z}\right)I(y,z)_{,z} \tag{7c}$$

$$+ \frac{z^l}{h^l}C_{44}^{(l)}(V_{,z} + W_{,y})I(y,z)_{,y} + 0.5P(\mathrm{i}kU_{,z} + k^2 W)I(y,z) = -\frac{z^l \rho^{(l)}\omega^2 W}{h^l}I(y,z)$$

where subscript comma indicates partial derivative.

In order to solve the coupled wave equations (7), we expand $U(y,z)$, $V(y,z)$ and $W(y,z)$ into products of two Legendre orthogonal polynomial series as

$$U(y,z) = \sum_{m,j=0}^{\infty} p_{m,j}^1 Q_m(z)Q_j(y), \quad V(y,z) = \sum_{m,j=0}^{\infty} p_{m,j}^2 Q_m(z)Q_j(y),$$

$$W(y,z) = \sum_{m,j=0}^{\infty} p_{m,j}^3 Q_m(z) Q_j(y), \tag{8}$$

where $p_{m,j}^i (i = 1,2,3)$ are the expansion coefficients and

$$Q_m(z) = \sqrt{\frac{2m+1}{h}} P_m \left(\frac{2z-h}{h} \right), \quad Q_j(y) = \sqrt{\frac{2j+1}{d}} P_j \left(\frac{2y-d}{d} \right) \tag{9}$$

with P_m and P_j being the mth and the jth Legendre polynomial. Theoretically, m and j run from 0 to ∞. However, in practice the summation over the polynomials in Eq. (8) can be truncated at some finite values $m = M$ and $j = J$, when the effects of higher order terms become negligible.

Multiplying Eq. (7) by $Q_n^*(z) \cdot Q_s^*(y)$ with n and s running respectively from 0 to M and from 0 to J, and integrating over z from 0 to h and over y from 0 to d, and taking advantage of the orthonormality of the polynomials, we can convert Eq. (7) into the forms:

$${}^l A_{11}^{j,m} p_{m,j}^1 + {}^l A_{12}^{j,m} p_{m,j}^2 + {}^l A_{13}^{j,m} p_{m,j}^3 = -\omega^2 \cdot {}^l M_{m,j} p_{m,j}^1, \tag{10a}$$

$${}^l A_{21}^{j,m} p_{m,j}^1 + {}^l A_{22}^{j,m} p_{m,j}^2 + {}^l A_{23}^{j,m} p_{m,j}^3 = -\omega^2 \cdot {}^l M_{m,j} p_{m,j}^2, \tag{10b}$$

$${}^l A_{31}^{j,m} p_{m,j}^1 + {}^l A_{32}^{j,m} p_{m,j}^2 + {}^l A_{33}^{j,m} p_{m,j}^3 = -\omega^2 \cdot {}^l M_{m,j} p_{m,j}^3, \tag{10c}$$

where ${}^l A_{\alpha\beta}^{j,m} (\alpha, \beta = 1,2,3)$ and ${}^l M_{m,j}$ are the elements of the non-symmetric matrices A and M, which can be obtained by using Eq. (7).

Eq. (10) can be rewritten as

$$\begin{bmatrix} {}^l A_{11}^{j,m} & {}^l A_{12}^{j,m} & {}^l A_{13}^{j,m} \\ {}^l A_{21}^{j,m} & {}^l A_{22}^{j,m} & {}^l A_{22}^{j,m} \\ {}^l A_{31}^{j,m} & {}^l A_{32}^{j,m} & {}^l A_{33}^{j,m} \end{bmatrix} \begin{Bmatrix} p_{m,j}^1 \\ p_{m,j}^2 \\ p_{m,j}^3 \end{Bmatrix} = -\omega^2 \begin{bmatrix} {}^l M_{m,j} & 0 & 0 \\ 0 & {}^l M_{m,j} & 0 \\ 0 & 0 & {}^l M_{m,j} \end{bmatrix} \begin{Bmatrix} p_{m,j}^1 \\ p_{m,j}^2 \\ p_{m,j}^3 \end{Bmatrix}. \tag{11}$$

So, Eq. (11) forms the eigenvalue problem to be solved. The eigenvalue ω^2 gives the angular frequency of the guided wave, and the eigenvectors $p_{m,j}^i (i = 1,2,3)$ allow the displacement components to be calculated. By using the relation $Vph = \omega/k$, the phase velocity can be obtained.

3   Numerical results and discussions

The Voigt-type model is used in this study to calculate the effective parameters of the FGM rod, which can be expressed as

$$C(z) = C_1 V_1(z) + C_2 V_2(z), \tag{12}$$

where C_i and $V_i(z)$ denote the ith material property and the corresponding volume fraction, respectively, and $\sum V_i(z) = 1$. Then we can express the material properties of the FGM as

$$C(z) = C_2 + (C_1 - C_2)V_1(z). \tag{13}$$

According to Eq. (5), we express the gradient profile of the material volume fraction as a power series expansion. By the Mathematica function 'Fit', the coefficients of the power series can be determined.

3.1 Comparison with the reference solution

In order to validate the effectiveness of the present approach and our computer program, we calculate a rectangular rod with $h = 16$ mm and $d = 5$ mm, The material is aluminum and the elastic coefficients are $C_{11} = C_{22} = C_{33} = 107.8$ GPa, $C_{12} = C_{13} = C_{23} = 54.94$ GPa, $C_{44} = C_{55} = C_{66} = 26.45$ GPa and the density is $\rho = 2700$ kg/m^3. Dispersion curves are given in Fig. 2, where lines are results from Loveday (2006), and dotted lines are results from the present approach. It is easily found that the results from the present approach agree well with the reference data.
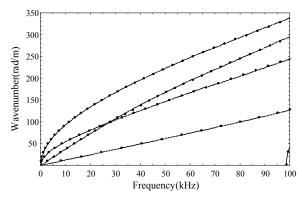

Figure 2: Dispersion curves for a rectangular aluminum rod; lines: Philip W. Loveday's results, dotted lines: the authors' results.

Table 1: The material properties of the FGM rod (C_{ij} (10^9 N/m^2), ρ (kg/m^3)).

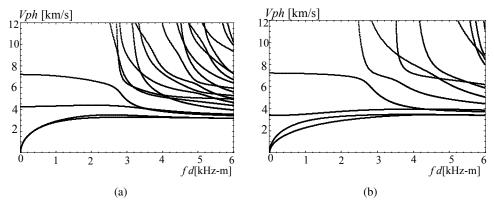| Property	C_{11}	C_{22}	C_{33}	C_{12}	C_{13}	C_{23}	C_{44}	C_{55}	C_{66}	ρ
Steel	282	282	282	113	113	113	84	84	84	7932
Silicon Nitride	380	380	380	120	120	120	130	130	130	2370

Figure 3: Phase velocity dispersion curves for linearly graded rectangular rods: (a) $d/h = 1$, (b) $d/h = 2$.
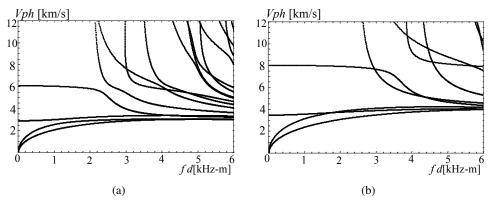

Figure 4: Phase velocity dispersion curves for graded rectangular rods with $d/h = 2$: (a) cubically graded rod, (b) sinusoidally graded rod.

3.2   Guided waves in FGM rectangular rods

In this section, we take the ceramic-metal FGM structure as an example to discuss the guided wave characteristics. The FGM rod is composed of steel (bottom surface) and silicon nitride, and the corresponding material parameters are given in Table 1. Firstly, we discuss various FGM rods to illustrate the influences of the width to height ratio and gradient functions on the guided wave charateristics. Four FGM rectangular rods are considered: (a) linearly graded rod with $V_1(z) = z$ and $d/h = 1$; (b) linearly graded rod with $V_1(z) = z$ and $d/h = 2$; (c) cubically graded rod with $V_1(z) = z^3$ and $d/h = 2$; (d) sinusoidally graded rod with $V_1(z) = \sin(z)$ and $d/h = 2$. The corresponding phase velocity dispersion curves are shown in

Figs. 3 and 4. It can be observed that the FGM rod has no cut-off frequencies for the first four wave modes. which is different from the infinite graded plate where the first three modes have no cut-off frequencies. The reason lies in that there are two finite dimensions in the rod but only a finite dimension in the plate. Furthermore, both width to height ratio and gradient function have significant influences on the dispersion curves. With increasing the width to height ratio, the difference between the first mode dispersion curve for the linearly graded rectangular rods and the second one becomes more significant at low frequency.

Next, a special structure, a sinusoidally graded square rod, is considered. From both geometrically and material distributions, the problem is symmetric with respect to both y- and z-axis. Fig. 5 presents its phase velocity dispersion curves. We can see that the dispersion curves of the first two modes are coincident. The displacement distributions are shown in Figs. 6 and 7 for the first two wave modes at $kd = 3$. For the first mode, the displacement distribution in wave propagating direction (the displacement u) is symmetric with respect to y-axis but anti-symmetric to z-axis. The other two displacement components v and w are respectively anti-symmetric and symmetric with respect to y- and z-axis. The displacement distribution of the second mode is in contrast to that of the first mode. Its displacement u is anti-symmetric with respect to y-axis but symmetric to z-axis. The displacement components v and w are respectively symmetric and anti-symmetric with respect to y- and z-axis.
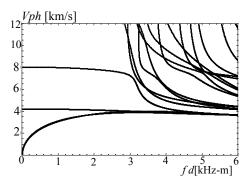

Figure 5: Phase velocity dispersion curves for the sinusoidally graded square rod.

The displacement distributions of guided waves at high frequencies are also investigated. Figs. 8 and 9 show the displacement distributions of the second mode for the linearly graded rectangular rod with $d/h = 2$ and sinusoidally graded rectangular rod with $d/h = 2$ at $kd = 6000$. It is easily discovered that the displacements are mainly concentrated in the vicinity of the four rod outer surfaces. For the linearly
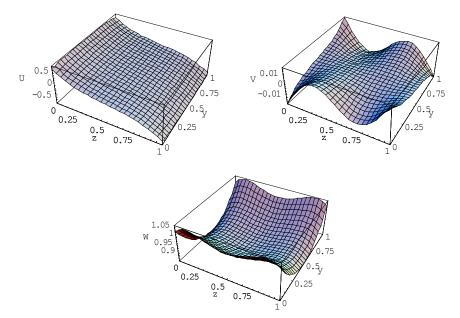
Figure 6: Displacement profiles of the first mode for the sinusoidally graded square rod at $kd = 3$.
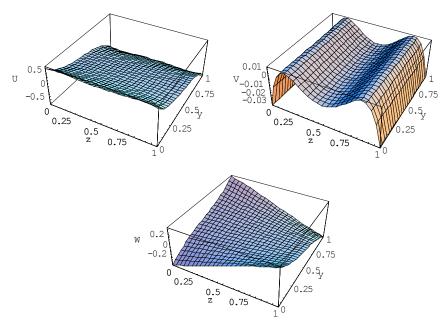

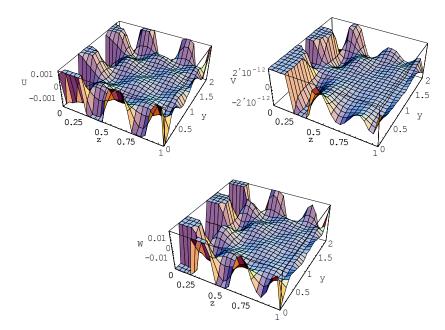Figure 7: Displacement profiles of the second mode for the sinusoidally graded square rod at $kd = 3$.

Figure 8: Displacement profiles of the second mode for the linearly graded rectangular rod with $d/h = 2$ at $kd = 6000$.
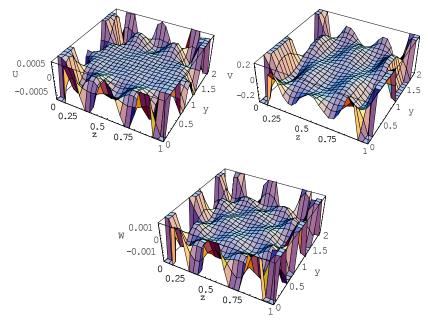

Figure 9: Displacement profiles of the second mode for the sinusoidally graded rectangular rod with $d/h = 2$ at $kd = 6000$.

graded rod, the displacements are more localized near the bottom surface, while for the sinusoidally graded rod, the displacements are more concentrated around the bottom and top surfaces. This means that the guided waves at high frequencies propagate predominantly near the side with more steel phase. The reason lies in the fact that the wave speed of the steel is lower than that of the silicon nitride.
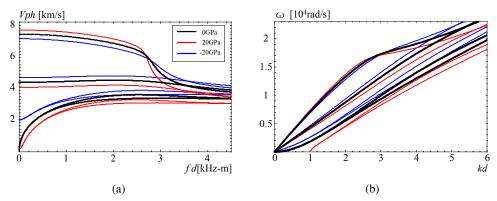

Figure 10: Dispersion curves for the linearly graded square rods with initial stress: (a) frequency spectra; (b) phase velocity spectra.
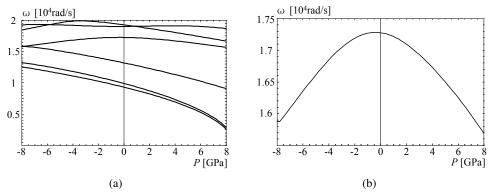

Figure 11: Variation of the frequency with respect to initial stress for the linearly graded square rods: (a) at $kh = 3$; (b) the forth order mode at $kh = 3$.

Fig. 10 shows the frequency spectra and phase velocity spectra of the first four order modes for the linearly graded square rods with different homogeneous initial stresses. The curves reveal that the initial stress has a pronounced effect on the dispersion curves. The effects of the compressive stress are contrary to those of the stretch stress, and the effects are different for different modes. For the first three

modes, a compressive stress makes the wave speed lower and a stretch stress makes the wave speed higher. But a compressive stress makes the wave speed higher at low frequencies for the forth modes. The effects of the initial stress on the dispersion curves are significant and become strong with the wavenumber increasing.

Fig. 11 illustrates the variation of the frequency with respect to initial stress for the linearly graded square rods. We can notice that the relations of frequency vs. initial stress are nonlinear and the varying trends of each mode are different. The effects of the compressive stress and stretch stress are not always contrary. Like the forth order mode, as showed in Fig. 11(b), the biggest frequency is at about initial stress $P = 0$, both the compressive stress and stretch stress make the wave speed and frequency lower.
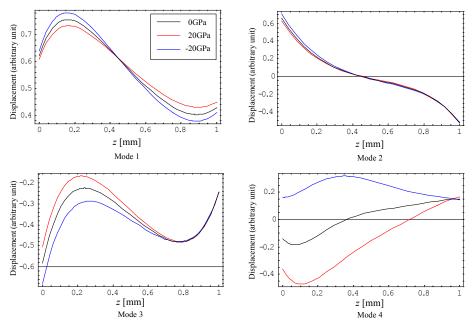

Figure 12: u displacement distributions at $y = 0$ for the first four modes of the linearly graded square rod with initial stress.

Figs. 12 and 13 show the effects of the initial stress on the one dimensional u displacement distributions at $z = 0$ and $y = 0$ for the first four modes of the linearly graded square rods, respectively. We can notice that the effects of initial stress on the u displacement distribution of the different modes are different, and the effects of compressive stress and the stretch stress are contrary. At $y = 0$, the effect is very small on the second mode and big on other three modes, and the effect is very
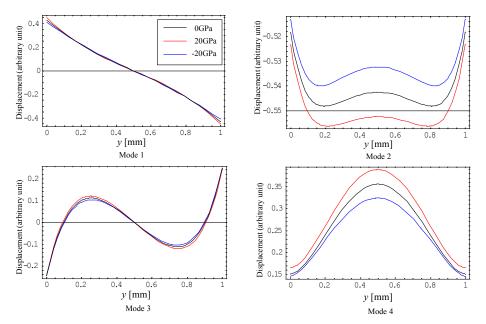
Figure 13: *u* displacement distributions at $z = 0$ for the first four modes of the linearly graded square rod with initial stress.

significant for high modes. At $z = 0$, the effect is very small on the first and third modes and strong on other two modes.

4 Conclusions

An extended orthogonal polynomial approach is used to investigate the guided waves propagation in functionally graded rods with rectangular cross-section under initial stress based on the "Mechanics of Incremental Deformations". Numerical comparison of the dispersion curves with reference solutions shows that the present approach is appropriate to solve the guided wave propagation problems in 2-D FGM structures. The dispersion curves and displacement distributions of various FGM rectangular rods are illustrated. Numerical examples indicate that both the width to height ratio and the gradient function have significant influences on the guided wave charateristics, and guided waves at high frequencies propagate predominantly around the side with the material having lower wave speed. The effects of the initial stress on the phase velocity dispersion curves are significant and become strong with the wavenumber increasing. The effects of the compressive stress are usually contrary to those of the stretch stress. The variation of the frequency with respect to initial stress is nonlinear and the varying trend of each

mode is different.

All these results can give theoretical guidance for nondestructive evaluation using the ultrasonic wave generation devices, and we believe that the present approach would be of interest in nondestructive testing evaluation and can deal with multi-field coupled 2D structures and 2D structures with more complex cross sections.

References

Abd-Alla, A. M.; Ahmed, S. M. (1999): Propagation of Love waves in a non-homogeneous orthotropic elastic layer under initial stress overlying semi-infinite medium. *Applied Mathematics and Computation*, vol. 106, no. 2, pp. 265–275.

Biot M.A. (1965): Mechanics of Incremental Deformations, John Wiley & Sons, Inc., New York, 1965.

Bishay, P. L.; Sladek, J.; Sladek, V.; Atluri, S. N. (2012): Analysis of functionally graded magneto-electro-elastic composites using hybrid/mixed finite elements and node-wise material properties. *Cmc: Computers Materials & Continua*, vol. 29, no. 3, pp. 213–261.

Chakraborty, A.; Gopalakrishnan, S. (2004): A higher-order spectral element for wave propagation analysis in functionally graded materials. *Acta Mechanica*, vol. 172, no. 1, pp. 17–43.

Chen, W. Q.; Wang, H. M.; Bao; R. H. (2007): On calculating dispersion curves of waves in a functionally graded elastic plate. *Composite Structures*, vol. 81, no. 2, pp. 233–242.

Elmaimouni, L.; Lefebvre, J.E.; Zhang, V.; Gryba, T. (2005): Guided waves in radially graded cylinders: A polynomial approach. *NDT&E International*, vol. 38, no. 3, pp. 344–353.

Liu, G. R.; Tani, J.; Ohyoshi, T. (1991): Lamb waves in a functionally gradient material plate and its transient response, Part 1: Theory, Part 2: Calculation results. *Transactions of the Japan Society of Mechanical Engineering*, vol. 57(A), pp. 603–611.

Han, X.; Liu, G. R. (2003): Elastic waves propagating in a functionally graded piezoelectric cylinder. *Smart Materials & Structures*, vol. 12, no. 6, pp. 962–971.

Han, X.; Liu, G. R.; Lam, K. Y. (2000): A quadratic layer element for analyzing stress waves in FGMs and its application in material characterization. *Journal of Sound and Vibration*, vol. 236, no. 2, pp. 307–321.

Hosseini, S. M. (2009): Coupled thermoelasticity and second sound in finite length functionally graded thick hollow cylinders (without energy dissipation). *Materials and Design*, vol. 30, no. 6, pp. 2011–2023.

Lefebvre, J. E.; Zhang, V.; Gazalet, J.; Gryba, T.; Sadaune, V. (2001): Acoustic wave propagation in continuous functionally graded plates: An extension of the Legendre polynomial approach. *IEEE Transactions On Ultrasonics, Ferroelectrics, and Frequency Control*, vol. 48, no. 5, pp. 1332–1340.

Liu, Y. J.; Han, Q.; Huang, H. W.; Li, C. L.; Liu, X. C.; Wu, B. (2015): Computation of dispersion relations of functionally graded rectangular bars. *Composite Structures*, vol. 133, no. 1, pp. 31–38.

Loveday, P. W. (2006): Numerical comparison of patch and sandwich piezoelectric transducers for transmitting ultrasonic waves. *Smart Structures and Materials 2006: Modeling, Signal Processing and Control, Proceedings of SPIE*, vol. 6166, pp. 1–8.

Moussavinezhad, S. M.; Shahabian, F.; Hosseini, S. M. (2013): Two-dimensional elastic wave propagation analysis in finite length FG thick hollow cylinders with 2D nonlinear grading patterns using MLPG method. *CMES: Computer Modeling in Engineering and Sciences*, vol. 91, no. 3, pp. 177–204.

Qian, Z. H.; Jin, F.; Lu, T. J.; Kishimoto, K.; Hirose, S. (2010): Effect of initial stress on Love waves in a piezoelectric structure carrying a functionally graded material layer. *Ultrasonics*, vol. 50, no. 1, pp. 84–90.

Saroj, P. K.; Sahu, S. A.; Chaudhary, S.; Chattopadhyay, A. (2015): Love-type waves in functionally graded piezoelectric material (FGPM) sandwiched between initially stressed layer and elastic substrate. *Waves in Random and Complex Media*, vol. 25, no. 4, pp. 608–627.

Sun, D.; Luo, S. N. (2011): Wave propagation and transient response of a FGM plate under a point impact load based on higher-order shear deformation theory. *Composite Structures*, vol. 93, no. 5, pp. 1474–1484.

Xue, C. X.; Pan, E. (2013): On the longitudinal wave along a functionally graded magneto-electro-elastic rod. *International Journal of Engineering Science*, vol. 62, pp. 48–55.

Yu, J. G.; Ratolojanahary, F. E.; Lefebvre; J. E. (2011): Guided waves in functionally graded viscoelastic plates. *Composite Structures*, vol. 93, no. 11, pp. 2671–2677.

Yu, J. G.; Wu, B.; He, C. F. (2007): Characteristics of guided waves in graded spherical curved plates. *International Journal of Solids and Structures*, vol. 44, no. 11–12, pp. 3627–3637.

Yu, J. G.; Zhang, C. Z. (2013): Influences of initial stresses on guided waves in functionally graded hollow cylinders. *Acta Mechanica*, vol. 224, no. 4, pp. 745–757.

Yu, J. G.; Zhang, C. Z. (2014): Effects of initial stress on guided waves in orthotropic functionally graded plates. *Applied Mathematical Modelling*, vol. 38, no. 2, pp. 464–478.

Zhu, J.; Yang, J.; Kitipornchai, S. (2013): Dispersion spectrum in a functionally graded carbon nanotube-reinforced plate based on first-order shear deformation plate theory. *Composites Part B-Engineering*, vol. 53, pp. 274–283.